

The Minimum Barrier Distance

Robin Strand^a, Krzysztof Chris Ciesielski^{b,c}, Filip Malmberg^a, Punam K. Saha^d

^a*Centre for Image Analysis, Uppsala University, Sweden*

^b*Department of Mathematics, West Virginia University, Morgantown, WV 26506-6310, USA*

^c*Department of Radiology, MIPG, University of Pennsylvania, Blockley Hall – 4th Floor, 423 Guardian Drive, Philadelphia, PA 19104-6021, USA*

^d*Department of Electrical and Computer Engineering and the Department of Radiology, The University of Iowa, Iowa City, IA 52242, USA*

Abstract

In this paper we introduce a minimum barrier distance, MBD, defined for the (graphs of) real-valued bounded functions f_A , whose domain D is a compact subsets of the Euclidean space \mathbb{R}^n . The formulation of MBD is presented in the continuous setting, where D is a simply connected region in \mathbb{R}^n , as well as in the case where D is a digital scene. The MBD is defined as the minimal value of the barrier strength of a path between the points, which constitutes the length of the smallest interval containing all values of f_A along the path.

We present several important properties of MBD, including the theorems: on the equivalence between the MBD ρ_A and its alternative definition φ_A ; and on the convergence of their digital versions, $\widehat{\rho}_A$ and $\widehat{\varphi}_A$, to the continuous MBD $\rho_A = \varphi_A$ as we increase a precision of sampling. This last result provides an estimation of the discrepancy between the value of $\widehat{\rho}_A$ and of its

Email addresses: robin@cb.uu.se (Robin Strand), KCies@math.wvu.edu (Krzysztof Chris Ciesielski), filip@cb.uu.se (Filip Malmberg), punam-saha@uiowa.edu (Punam K. Saha)

27 approximation $\widehat{\varphi}_A$. An efficient computational solution for the approxima-
28 tion $\widehat{\varphi}_A$ of $\widehat{\rho}_A$ is presented. We experimentally investigate the robustness of
29 MBD to noise and blur, as well as its stability with respect to the change
30 of a position of points within the same object (or its background). These
31 experiments are used to compare MBD with other distance functions: fuzzy
32 distance, geodesic distance, and max-arc distance. A favorable outcome for
33 MBD of this comparison suggests that the proposed minimum barrier dis-
34 tance is potentially useful in different imaging tasks, such as image segmen-
35 tation.

36 *Keywords:* Image processing, Distance function, Distance transform,
37 Fuzzy subset, Path strength

38 1. Introduction

39
40 Over the past several decades, distance transform (DT) [1, 2, 3, 4, 5, 6, 7]
41 has been widely used as an effective tool for analyzing object morphology and
42 geometry [8, 9, 10]. Most DT measures described in the literature essentially
43 capture the Euclidean distance of a candidate point from a target set, often
44 the background. Rosenfeld and Pfaltz [11] introduced the simple yet funda-
45 mental idea that, in a digital grid, the global Euclidean distance transform
46 may be approximated by propagating local distances between neighboring
47 pixels. Borgefors [2, 3] extensively studied DTs for binary objects includ-
48 ing the popular algorithm [2] that computes DT by using different local
49 step lengths for different types of neighbors. Also, she studied the geome-
50 try and equations of 3D DT and presented a two-pass raster scan algorithm
51 for computing approximate Euclidean distance transform [3]. An algorithm

53 for computing in linear time the exact Euclidean distance transform for the
54 rectangular digital images was described in [12] and elaborated on in [13].

55 Other authors have considered distance functions where the image data
56 is taken into account, see, e.g., [5, 14, 15, 16]. Distance transforms for such
57 distance functions are typically computed on discrete sets using variations on
58 Dijkstra’s algorithm. Falcão et al. showed that this method of computation
59 can be used for any *smooth* distance function, as defined in [16].

60 Image processing on fuzzy subsets has gained a lot attention, [9, 10, 17,
61 18]. It provides a flexible framework for handling uncertainty, arising from
62 sampling artifacts, illumination inhomogeneities and other imperfections in
63 the image representation and acquisition process. Fuzzy sets are defined
64 using a membership function which gives the degree of belongingness with
65 respect to some set.

66 In this paper, we introduce a distance function defined for the real-valued
67 bounded functions f_A (so, in particular, for fuzzy sets), whose domain D is a
68 compact subsets of the Euclidean space \mathbb{R}^n . We refer to the new distance as
69 the “minimum barrier distance” and study its properties in the continuous
70 setting, where D is a simply connected region in \mathbb{R}^n , as well as in the case
71 where D is a digital scene. In image processing and computer vision, ordi-
72 nary and fuzzy distance functions [1, 2, 3, 4, 5, 6, 11, 14, 15, 16] have widely
73 been used to represent a spatial relation between each pair of points in a
74 Euclidean space or a fuzzy subset. For example, ordinary distance function,
75 commonly used for binary images, is a measure of the shortest digital path
76 length between two points while, as viewed by Saha et al. [5], fuzzy distance
77 is a measure of the “minimum material to be traversed” to move from one
78

79 point to the other where the fuzzy membership function is linked to local
80 material density. Under both ordinary and fuzzy distance frameworks, the
81 length of a path strictly increases as the path grows. The formulation of min-
82 imum barrier distance function possesses the following property: The length
83 of a path may remain constant during its growth until a new stronger barrier
84 is met on the path. This subtle shift in the notion of path length allows the
85 new distance function to capture separation between two points in the sense
86 of “connectivity” [19] in a fuzzy set unlike geometric properties commonly
87 represented by existing distance functions. Thus, it may be an interesting
88 avenue to study strengths and limitations of the new function that theoret-
89 ically behaves like a distance while resembling to “anti-connectivity” from a
90 user perspective. For example, the new distance may be useful to determine
91 minimum barrier to move from one region to another and also, to locate the
92 minimum barrier path. In the context of image processing and computer
93 vision, the new distance function may be useful in image segmentation and
94 region growing.

95 We show that (pseudo-)metric properties of the “minimum barrier dis-
96 tance” are maintained by its formulation in a digital grid. We give examples
97 that show that the minimum-barrier distance cannot be computed using the
98 standard Dijkstra algorithm mentioned above. Instead, we give an approx-
99 imation of the new distance measure for fuzzy subsets on digital grids and
100 show that the minimum barrier distance over a continuous fuzzy subset can
101 be approximated arbitrarily close in a digital grid by using a sufficiently dense
102 sampling grid. A similar approximation idea is presented in [20]. An effi-
103 cient computational solution for the minimum barrier distance is presented

104

105 using the approximation. The experiments show that the minimum barrier
 106 distance is robust to noise, blur, and seed point position.

107 2. The Minimum Barrier Distance in \mathbb{R}^n

108 Let $f_A: D \rightarrow \mathbb{R}$ be any bounded function and let A be its graph, that is,
 109

$$110 A = \{(x, f_A(x)) : x \in D\}.$$

111 We will concentrate on the functions $f_A: D \rightarrow [0, 1]$, in which case A will be
 112 treated as a fuzzy subset of D and f_A will be referred to as the *membership*
 113 *function* of A in D . However, the presented material works for mappings f_A
 114 with any bounded range. For example, $f_A(x)$ could be the intensity value at
 115 x in a digital image.

116 For $D \subset \mathbb{R}^n$ and $p, q \in D$, a *path from p to q* (in D) is any continuous
 117 function $\pi: [0, 1] \rightarrow D$ with $p = \pi(0)$ and $q = \pi(1)$. We use the symbol $\Pi_{p,q}$
 118 (or just Π , when p and q are clear from the context) to denote the family
 119 of all such paths. Recall, that $D \subset \mathbb{R}^n$ is *path connected* provided for every
 120 $p, q \in D$ there exists a path $\pi: [0, 1] \rightarrow D$ from p to q .

121 The goal of this section is to introduce and discuss the following notion of
 122 the minimum barrier distance defined for the bounded continuous functions
 123 $f_A: D \rightarrow \mathbb{R}$ in the case when $D \subset \mathbb{R}^n$ is path connected.
 124

125 **Definition 1.** For a path $\pi: [0, 1] \rightarrow D$, the *barrier* along π is defined as

$$126 \tau_A(\pi) = \max_t f_A(\pi(t)) - \min_t f_A(\pi(t)) = \max_{t_0, t_1} (f_A(\pi(t_1)) - f_A(\pi(t_0))). \quad (1)$$

127 The *minimum barrier distance* $\rho_A: D \times D \rightarrow [0, \infty)$ for a path connected
 128 $D \subset \mathbb{R}^n$ is defined via formula

$$129 \rho_A(p, q) = \inf_{\pi \in \Pi_{p,q}} \tau_A(\pi). \quad (2)$$

131
 132
 133
 134
 135
 136
 137
 138
 139
 140
 141
 142
 143
 144
 145
 146
 147
 148
 149
 150
 151
 152
 153
 154
 155
 156

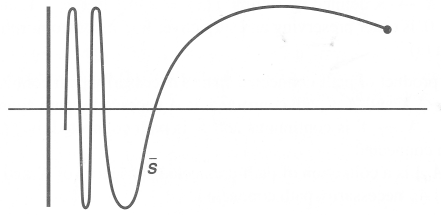


Figure 1: Topologists sine curve from Example 1

Notice that the maxima and minima in the formula (1) are attained (by the Extreme Value Theorem), since the composition function $f_A \circ \pi$ is continuous. At the same time, the next example shows that a path that defines the minimum barrier distance ρ_A is not always attained, that is, the infimum operation in the definition (2) cannot be replaced with the minimum operation.

Example 1. Let $D = [-1, 1]^2$ and T be the topologists sine curve, that is, T is the closure of the set $S = \{\langle x, \sin(1/x) \rangle : x \in (0, 1]\}$, see Figure 1. If $f_A(x)$ is defined as the Euclidean distance from $x \in D$ to T , then f_A is continuous. If $p = \langle 0, 0 \rangle$ and $q = \langle 1, \sin 1 \rangle$, then $\inf_{\pi \in \Pi_{p,q}} \tau_A(\pi) = 0$, but $\tau_A(\pi) > 0$ for any $\pi \in \Pi$ (since T is not path connected).

Notice that $\rho_A(p, q)$ is related to the geodesic distance $g_A(p, q)$ between the points $\langle p, f_A(p) \rangle$ and $\langle q, f_A(q) \rangle$ along the surface A . Actually, $\rho_A(p, q)$ is, in a way, a vertical component of $g_A(p, q)$, so that $\rho_A(p, q) \leq g_A(p, q)$.

Definition 2. A function $d: D \times D \rightarrow [0, \infty)$ is a *metric* on a set D provided, for every $x, y, z \in D$,

- (i) $d(x, x) = 0$ (identity)

157 (ii) $d(x, y) > 0$ for all $x \neq y$ (positivity)

158 (iii) $d(x, y) = d(y, x)$ (symmetry)

159 (iv) $d(x, z) \leq d(x, y) + d(y, z)$ (triangle inequality)

160 A function d that obeys properties (i), (iii), and (iv) is called a *pseudo-metric*.

161 In the proof that ρ_A is a pseudo-metric, we will use the following notion.
162 The *concatenation* $\pi_1 \cdot \pi_2$ of the paths π_1 and π_2 such that $\pi_1(1) = \pi_2(0)$ is

$$(\pi_1 \cdot \pi_2)(t) = \begin{cases} \pi_1(2t) & \text{if } t \in [0, 1/2] \\ \pi_2(2t) & \text{otherwise.} \end{cases}$$

163 **Remark 1.** If $\pi_1(1) = \pi_2(0)$, then $\tau_A(\pi_1) + \tau_A(\pi_2) \geq \tau_A(\pi_1 \cdot \pi_2)$.

164 **Proposition 1.** ρ_A is a pseudo-metric.

165 *Proof.* It is obvious that ρ_A is non-negative and symmetric. It satisfies the
166 identity property (i), since for the constant path π_x defined via $\pi_x(t) = x$ for
167 all $t \in [0, 1]$, we have $\rho_A(x, x) \leq \tau_A(\pi_x) = f_A(x) - f_A(x) = 0$.

168 Now we prove the triangular inequality. Given three arbitrary points
169 $p, q, r \in D$ and an $\varepsilon > 0$ chose the paths $\pi_{p,q} \in \Pi_{p,q}$ and $\pi_{q,r} \in \Pi_{q,r}$ such that
170 $\rho_A(p, q) \geq \tau(\pi_{p,q}) - \varepsilon$ and $\rho_A(q, r) \geq \tau(\pi_{q,r}) - \varepsilon$. Then, using Remark 1, we
171 have

$$\rho_A(p, q) + \rho_A(q, r) \geq \tau(\pi_{p,q}) - \varepsilon + \tau(\pi_{q,r}) - \varepsilon \geq \tau_A(\pi_{p,q} \cdot \pi_{q,r}) - 2\varepsilon \geq \rho_A(p, r) - 2\varepsilon.$$

172 Since the inequality $\rho_A(p, q) + \rho_A(q, r) \geq \rho_A(p, r) - 2\varepsilon$ holds for an arbitrary
173 $\varepsilon > 0$, we must also have $\rho_A(p, q) + \rho_A(q, r) \geq \rho_A(p, r)$, as required. \square

183 Notice that for a constant function f_A we have $\rho_A \equiv 0$, so the property
 184 (ii) does not hold. In particular, in general, ρ_A is not a metric.

185 Now, consider the following alternative definition φ_A of the function ρ_A .
 186 In Theorem 1 we prove that under the very mild assumptions on the set D ,
 187 which include all convex subsets of \mathbb{R}^n (so, also, the rectangular regions), the
 188 mappings φ_A and ρ_A are identical. This gives a tool for approximating ρ_A in
 189 the digital space considered in Section 3.

190 **Definition 3.** Define the mapping $\varphi_A: D \times D \rightarrow [0, \infty)$ via formula

$$191 \quad \varphi_A(p, q) = \inf_{\pi_1 \in \Pi_{p,q}} \max_t f_A(\pi_1(t)) - \sup_{\pi_0 \in \Pi_{p,q}} \min_t f_A(\pi_0(t)).$$

193 Note that φ_A is defined by two separate paths. Also, as in the case of ρ_A ,
 194 the minimum/maximum over numbers $t \in [0, 1]$ exists, while neither infimum
 195 not supremum operators can be replaced by maximum/minimum.

196 Recall, that a set $D \subset \mathbb{R}^n$ is *simply connected*, provided it is path con-
 197 nected and for all $p, q \in D$ the paths $\pi_0, \pi_1 \in \Pi_{p,q}$ are homotopic, that is,
 198 there exists a continuous function $h: [0, 1]^2 \rightarrow D$, known as a *homotopy* be-
 199 tween π_0 and π_1 , such that $h(\cdot, 0) = \pi_0(\cdot)$, $h(\cdot, 1) = \pi_1(\cdot)$, and $h(0, \cdot)$, $h(1, \cdot)$
 200 constant. Intuitively, the homotopy condition means that D has no holes.

201 The proof of Theorem 1 will be based on the following two lemmas, the
 202 first of which is illustrated in Figure 2.

203 **Lemma 1.** *Let F_0 and F_1 be a closed disjoint subsets of $[0, 1]^2$ such that*
 204 *$F_0 \setminus (0, 1)^2 \subset (0, 1) \times \{1\}$ and $F_1 \setminus (0, 1)^2 \subset (0, 1) \times \{0\}$. Then, there exists*
 205 *a continuous path $\bar{\pi}: [0, 1] \rightarrow [0, 1]^2 \setminus (F_0 \cup F_1)$ from $\langle 0, .5 \rangle$ to $\langle 1, .5 \rangle$.*

206 *Proof.* The sets $\bar{F}_0 = F_0 \cup (\mathbb{R} \times [1, \infty))$ and $\bar{F}_1 = F_1 \cup (\mathbb{R} \times (-\infty, 0])$ are
 207 disjoint and closed in \mathbb{R}^2 . Moreover, there is a path from $\langle 0, .5 \rangle$ to $\langle 1, .5 \rangle$ both
 208

209
 210
 211
 212
 213
 214
 215
 216
 217
 218
 219
 220
 221
 222
 223
 224
 225
 226
 227
 228
 229
 230
 231
 232
 233
 234

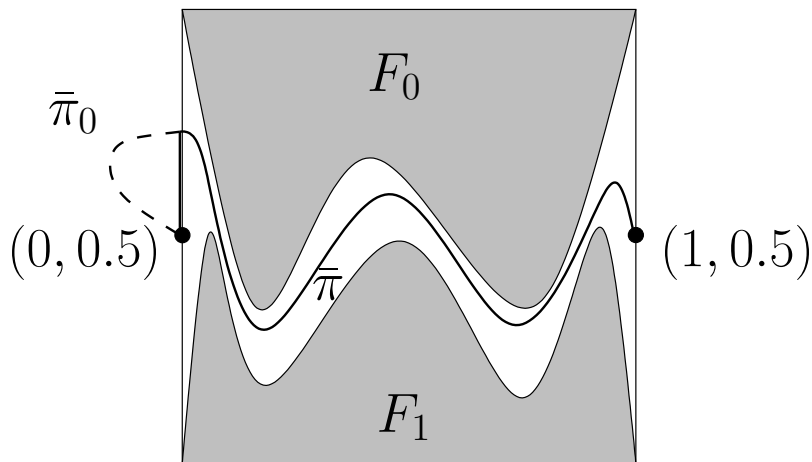


Figure 2: Illustration of Lemma 1. See the text for notation.

in $\mathbb{R}^2 \setminus \bar{F}_0$ (following the lower boundary of $[0, 1]^2$) and in $\mathbb{R}^2 \setminus \bar{F}_1$ (following the upper boundary of $[0, 1]^2$). Therefore, by a version of Alexander's lemma from [22, p. 137], there exists a path $\bar{\pi}_0: [0, 1] \rightarrow \mathbb{R}^2 \setminus (\bar{F}_0 \cup \bar{F}_1) \subset \mathbb{R} \times (0, 1)$ from $\langle 0, .5 \rangle$ to $\langle 1, .5 \rangle$. Now, if $r: \mathbb{R} \times (0, 1) \rightarrow [0, 1] \times (0, 1)$ is such that $r(x)$ is the point in $[0, 1] \times (0, 1)$ closest to x , then the continuous mapping $\bar{\pi} = r \circ \bar{\pi}_0: [0, 1] \rightarrow ([0, 1] \times (0, 1)) \setminus (F_0 \cup F_1)$ is as desired. \square

Lemma 2. *Let $D \subset \mathbb{R}^n$ be simply connected. For every $p, q \in D$ and $\varepsilon > 0$ there exists a $\pi \in \Pi_{p,q}$ such that $U_0 - \varepsilon < f_A(\pi(t)) < U_1 + \varepsilon$ for every $t \in [0, 1]$, where $U_0 = \sup_{\pi_0 \in \Pi_{p,q}} \min_t f_A(\pi_0(t))$ and $U_1 = \inf_{\pi_1 \in \Pi_{p,q}} \max_t f_A(\pi_1(t))$.*

Proof. Choose the paths $\pi_0, \pi_1 \in \Pi_{p,q}$ for which $\max_t f_A(\pi_1(t)) < U_1 + \varepsilon$ and $\min_t f_A(\pi_0(t)) > U_0 - \varepsilon$. Let $h: [0, 1]^2 \rightarrow D$ be a homotopy between the paths π_0 and π_1 . Define $F_0 = \{z \in [0, 1]^2: f_A(h(z)) \leq U_0 - \varepsilon\}$ and $F_1 = \{z \in [0, 1]^2: f_A(h(z)) \geq U_1 + \varepsilon\}$ and notice that they satisfy the assumptions of Lemma 1. (Typical position of sets F_0 and F_1 is shown in Figure 2. Function h is constant on each of the vertical segments of $[0, 1]^2$.)

Indeed, since functions $f_A \circ \pi_0$ and $f_A \circ \pi_1$ are continuous, the sets F_0 and F_1 are closed. They are disjoint, since $U_0 - \varepsilon < f_A(p) = f_A(\pi_0(0, t)) < U_1 + \varepsilon$ for every $t \in [0, 1]$. This inequality also implies that $F_0 \cup F_1$ is disjoint with $\{0\} \times [0, 1]$. Similarly, $F_0 \cup F_1$ is disjoint with $\{1\} \times [0, 1]$. Finally, F_0 is disjoint with $[0, 1] \times \{0\}$, as for any point $z = \langle t, 0 \rangle \in [0, 1] \times \{0\}$ we have $f_A(h(z)) = f_A(\pi_0(t)) > U_0 - \varepsilon$, and F_1 is disjoint with $[0, 1] \times \{1\}$, as $f_A(h(z)) = f_A(\pi_1(t)) < U_1 + \varepsilon$ for every $t \in [0, 1]$ and $z = \langle t, 1 \rangle \in [0, 1] \times \{1\}$.

Since the assumptions of Lemma 1 are satisfied, there exists a continuous path $\bar{\pi}: [0, 1] \rightarrow [0, 1]^2 \setminus (F_0 \cup F_1)$ from $\langle 0, .5 \rangle$ to $\langle 1, .5 \rangle$. Then the path $\pi = h \circ \bar{\pi}: [0, 1] \rightarrow D$ is as desired, since $\pi(0) = h(\bar{\pi}(0)) = h(0, .5) = h(0, 0) = \pi_0(0) = p$ and $\pi(1) = h(\bar{\pi}(1)) = h(1, .5) = h(1, 1) = \pi_1(1) = q$. Moreover, for every $t \in [0, 1]$ we have $f_A(\pi(t)) = f_A(h(\bar{\pi}(t))) \in (U_0 - \varepsilon, U_1 + \varepsilon)$, since otherwise $\bar{\pi}(t)$ is in $F_0 \cup F_1$, contradicting the choice of $\bar{\pi}$. \square

Theorem 1. *If $D \subset \mathbb{R}^n$ is simply connected, then the mappings ρ_A and φ_A are equal, that is, $\rho_A(p, q) = \varphi_A(p, q)$ for all $p, q \in D$.*

Proof. Fix $p, q \in D$ and an $\varepsilon > 0$. It is enough to prove the following two inequalities: $\varphi_A(p, q) \leq \rho_A(p, q) + \varepsilon$ and $\rho_A(p, q) \leq \varphi_A(p, q) + 2\varepsilon$. To prove the first of these, using the definition of ρ_A choose a $\pi \in \Pi_{p,q}$ for which $\rho_A(p, q) + \varepsilon \geq \tau_A(\pi)$. Then

$$\begin{aligned} \rho_A(p, q) + \varepsilon &\geq \tau_A(\pi) = \max_t f_A(\pi(t)) - \min_t f_A(\pi(t)) \\ &\geq \inf_{\pi_1 \in \Pi_{p,q}} \max_t f_A(\pi_1(t)) - \sup_{\pi_0 \in \Pi_{p,q}} \min_t f_A(\pi_0(t)) = \varphi_A(p, q), \end{aligned}$$

giving the required inequality $\varphi_A(p, q) \leq \rho_A(p, q) + \varepsilon$.

To prove the second inequality, use Lemma 2 to find a path $\pi \in \Pi_{p,q}$ for

261
 262
 263
 264
 265
 266
 267
 268
 269
 270
 271
 272
 273
 274
 275
 276
 277
 278
 279
 280
 281
 282
 283
 284
 285
 286

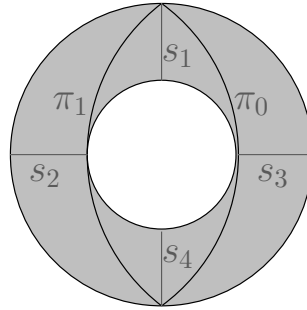


Figure 3: The domain $D = \{\langle x, y \rangle \in \mathbb{R}^2 : 1 \leq x^2 + y^2 \leq 4\}$ of $f_A(x, y) = \frac{x}{\sqrt{x^2 + y^2}}$ and the paths π_0 and π_1 from Example 2. Note that f_A is constant on the segments s_1, s_2, s_3, s_4 ; it attains the values: 0 on s_1 and s_4 , -1 on s_2 , and 1 on s_3 .

which the range of $f_A \circ \pi$ is contained in $(U_0 - \varepsilon, U_1 + \varepsilon)$. Then

$$\rho_A(p, q) \leq \tau_A(\pi) \leq (U_1 + \varepsilon) - (U_0 - \varepsilon) = \varphi_A(p, q) + 2\varepsilon,$$

finishing the proof. □

We will finish this section with a simple example of a continuous function $f_A: D \rightarrow [-1, 1]$ defined on a path connected, not simple connected, subset D of \mathbb{R}^2 for which the conclusion of Theorem 1 does not hold.

Example 2. Let $D = \{\langle x, y \rangle \in \mathbb{R}^2 : 1 \leq x^2 + y^2 \leq 4\}$, see Figure 3, and let $f_A: D \rightarrow [-1, 1]$ be defined via formula $f_A(x, y) = \frac{x}{\sqrt{x^2 + y^2}}$. (This is the cosine function of the argument of $\langle x, y \rangle$.) Let $p = \langle 0, 2 \rangle$ and $q = \langle 0, -2 \rangle$. Then, $\varphi_A(p, q) = 0$, as $\varphi_A(p, q) \leq \max_t f_A(\pi_1(t)) - \min_t f_A(\pi_0(t)) = 0$, where $\pi_1 \in \Pi_{p,q}$ is on the left hand side of the inner circle and $\pi_0 \in \Pi_{p,q}$ is the right hand side of this circle, see Figure 3. On the other hand, it is easy to see that $\rho_A(p, q) = 1$.

287 **3. The Minimum Barrier Distance in \mathbb{Z}^n**

288 In this section, we introduce a notion of the minimum barrier distance
 289 in digital setting, that is, for the bounded functions $\widehat{f}_A: \widehat{D} \rightarrow \mathbb{R}$, where \widehat{D}
 290 — a digital scene — is a finite subset of a digital space $\langle \phi\mathbb{Z}^n, \alpha \rangle$ defined as
 291 follows. \mathbb{Z} is the set of integers, $\phi > 0$ is a constant, $\phi\mathbb{Z}^n = \{\phi p: p \in \mathbb{Z}^n\}$,
 292 and α is an adjacency relation on $\phi\mathbb{Z}^n$. In what follows we will use the
 293 adjacency $\alpha = \alpha_1$, where, for $\kappa \in \{1, \dots, n-1\}$, two points in $\phi\mathbb{Z}^n$ are α_κ -
 294 adjacent provided at no coordinate they differ by more than ϕ and that the
 295 points differ in at most κ coordinates. Note that $\alpha = \alpha_1$ is equivalent to the
 296 standard 6-adjacency [23] in a 3D digital space; the theoretical formulations
 297 presented in the following is valid for α_κ for any other choice of κ , e.g., 18-
 298 or 26-adjacencies in 3D.

299 Recall, that a (digital) path in a subset \widehat{D} of $\langle \phi\mathbb{Z}^n, \alpha \rangle$ is any ordered
 300 sequence $\widehat{\pi} = \langle \widehat{\pi}(0), \widehat{\pi}(1), \dots, \widehat{\pi}(k) \rangle$ of points in \widehat{D} such that $\widehat{\pi}(i)$ is α -adjacent
 301 to $\widehat{\pi}(i-1)$ for all $i \in \{1, 2, \dots, k\}$; the path $\widehat{\pi}$ is from p to q when $\widehat{\pi}(0) = p$
 302 and $\widehat{\pi}(k) = q$. For a fixed set \widehat{D} , a family of all paths in \widehat{D} from p to q is
 303 denoted by $\widehat{\Pi}_{p,q}$ (or just $\widehat{\Pi}$, if p and q are clear from the context). Note that
 304 the digital paths are denoted by $\widehat{\pi}$, while the paths in the continuous space
 305 \mathbb{R}^n by π .

306 In what follows, we assume that the digital scenes \widehat{D} are of the rectangular
 307 form $\widehat{D}_\phi = D \cap \phi\mathbb{Z}^n$, where $D = \{x \in \mathbb{R}^n: L_i \leq x(i) \leq U_i\}$ for some real
 308 numbers L_i, U_i such that $L_i < U_i$ for all i . In particular, any two points in
 309 \widehat{D} are connected by a path.

310 In view of Theorem 1, there are two natural ways of defining the discrete
 311 minimum barrier distance for $\widehat{f}_A: \widehat{D} \rightarrow \mathbb{R}$, the discretization of the formulas
 312

for $\rho_A(p, q)$ and for $\varphi_A(p, q)$:

$$\widehat{\rho}_A(p, q) = \min_{\widehat{\pi} \in \widehat{\Pi}_{p,q}} \left(\max_i \left[\widehat{f}_A(\widehat{\pi}(i)) \right] - \min_j \left[\widehat{f}_A(\widehat{\pi}(j)) \right] \right), \quad (3)$$

$$\widehat{\varphi}_A(p, q) = \min_{\widehat{\pi}_1 \in \widehat{\Pi}_{p,q}} \max_i \left[\widehat{f}_A(\widehat{\pi}_1(i)) \right] - \max_{\widehat{\pi}_0 \in \widehat{\Pi}_{p,q}} \min_j \left[\widehat{f}_A(\widehat{\pi}_0(j)) \right]. \quad (4)$$

3.1. Properties of $\widehat{\rho}_A$ and $\widehat{\varphi}_A$

Proposition 2.

(i) Each of the functions $\widehat{\rho}_A$ and $\widehat{\varphi}_A$ is a pseudo-metric on \widehat{D} .

(ii) $\widehat{\varphi}_A(p, q) \leq \widehat{\rho}_A(p, q)$ for all $p, q \in \widehat{D}$. The equality need not hold.

(iii) The paths cost functions $\max_i \left[\widehat{f}_A(\widehat{\pi}_1(i)) \right]$ and $\min_j \left[\widehat{f}_A(\widehat{\pi}_0(j)) \right]$ are smooth in the sense of [16]. So, the transform $\widehat{\varphi}_A(p, \cdot)$ can be efficiently calculated by Dijkstra's algorithm.

However, the path cost function $\max_i \left[\widehat{f}_A(\widehat{\pi}(i)) \right] - \min_j \left[\widehat{f}_A(\widehat{\pi}(j)) \right]$ is not smooth in the sense of [16] and effective computing of the transform $\widehat{\rho}_A(p, \cdot)$ presents a challenge.

Proof. The proof of (i) is an easier version of that for Proposition 1.

To see (ii), choose $\widehat{\pi}$ with $\widehat{\rho}_A(p, q) = \max_i \left[\widehat{f}_A(\widehat{\pi}(i)) \right] - \min_j \left[\widehat{f}_A(\widehat{\pi}(j)) \right]$. Then the inequalities $\min_{\widehat{\pi}_1 \in \widehat{\Pi}_{p,q}} \max_i \left[\widehat{f}_A(\widehat{\pi}_1(i)) \right] \leq \max_i \left[\widehat{f}_A(\widehat{\pi}(i)) \right]$ and $\max_{\widehat{\pi}_0 \in \widehat{\Pi}_{p,q}} \min_j \left[\widehat{f}_A(\widehat{\pi}_0(j)) \right] \geq \min_j \left[\widehat{f}_A(\widehat{\pi}(j)) \right]$ imply

$$\widehat{\varphi}_A(p, q) \leq \max_i \left[\widehat{f}_A(\widehat{\pi}(i)) \right] - \min_j \left[\widehat{f}_A(\widehat{\pi}(j)) \right] = \widehat{\rho}_A(p, q).$$

An example that equality need not hold can be found in Figure 4.

(iii) Smoothness of the path cost functions for $\widehat{\varphi}_A(p, q)$ is easy to check and well known. (This was proved, for example, in [16].) Lack of such smoothness

339 for $\widehat{\rho}_A(p, q)$ can be seen in Figure 4: There is a unique $\widehat{\rho}_A$ -optimal path from
 340 the seed point to the upper right element, but its restriction to the first three
 341 elements is not $\widehat{\rho}_A$ -optimal. \square

342 Next we will prove, in Theorem 2, that if $\widehat{f}_A: \widehat{D}_\theta \rightarrow \mathbb{R}$ is a discretization
 343 of a continuous function f_A defined on a rectangular region D , then, for
 344 a sufficiently small ϕ , the numbers $\widehat{\varphi}_A(p, q)$ and $\widehat{\rho}_A(p, q)$ well approximate
 345 $\varphi_A(p, q) = \rho_A(p, q)$. Of course, in practice we do not have continuous images
 346 $f_A: D \rightarrow \mathbb{R}$, but the assumption is reasonable since most image acquisition
 347 methods induce smoothing of the image scene by a point spread function,
 348 see for example [24] for a discussion. Such an f_A can also be found by an
 349 interpolation of a digital function (often, just an image intensity function).
 350 We used this approach in our experiments presented in the next section.

351 In the proof of Theorem 2 we will need the following notion. The *hy-*
 352 *pervoxel* of a point p in $\phi\mathbb{Z}^n$ is the Voronoi region of p in \mathbb{R}^n , that is, the
 353 set $\{x \in \mathbb{R}^n: |x(i) - p(i)| \leq \phi/2 \text{ for all } i\}$. The *supercover digitization* in
 354 $\phi\mathbb{Z}^n$ of a subset A of \mathbb{R}^n , denoted $\mathcal{S}(A)$, is the union of all hypervoxels that
 355 meet the set A . The following simple fact can be found, for example, in [25].
 356 (Compare also [20].)

357 **Remark 2.** The supercover of any continuous path π in the rectangular
 358 region $D \subset \mathbb{R}^n$ (or, more precisely, of its image $\pi[0, 1] = \{\pi(t): t \in [0, 1]\}$)
 359 induces, in $\widehat{D}_\phi = D \cap \phi\mathbb{Z}^n$, an α -adjacent path $\widehat{\pi} = \langle \widehat{\pi}(0), \widehat{\pi}(1), \dots, \widehat{\pi}(k) \rangle$ with
 360 $\pi[0, 1] \subset \mathcal{S}(\{\widehat{\pi}(0), \widehat{\pi}(1), \dots, \widehat{\pi}(k)\})$ and $\{\widehat{\pi}(0), \widehat{\pi}(1), \dots, \widehat{\pi}(k)\} \subset \mathcal{S}(\pi[0, 1])$.
 361 In particular, the Hausdorff distance between the sets $\{\widehat{\pi}(0), \widehat{\pi}(1), \dots, \widehat{\pi}(k)\}$
 362 and $\pi[0, 1]$ is at most $\phi\sqrt{n}/2$, that is,
 363

- 365 • for every i there is a t with $\|\widehat{\pi}(i) - \pi(t)\| \leq \phi\sqrt{n}/2$ and, similarly, for
 366 every t there is an i with $\|\widehat{\pi}(i) - \pi(t)\| \leq \phi\sqrt{n}/2$.

367 **Theorem 2.** *Let D be a rectangular region in \mathbb{R}^n and $f_A: D \rightarrow \mathbb{R}$ be con-*
 368 *tinuous. Let $\widehat{\rho}_A$ and $\widehat{\varphi}_A$ be the discrete minimum barrier distance functions*
 369 *for the sampling \widehat{f}_A of f_A on \widehat{D}_ϕ , that is, with $\widehat{f}_A(p) = f_A(p)$ for all $p \in \widehat{D}_\phi$.*
 370 *Then, for every $\varepsilon > 0$ there exists a $\phi_0 > 0$ such that for every $\phi \in (0, \phi_0]$*

371 (•) $|\widehat{\rho}_A(p, q) - \rho_A(p, q)| < \varepsilon$ and $|\widehat{\varphi}_A(p, q) - \varphi_A(p, q)| < \varepsilon$ for all $p, q \in \widehat{D}_\phi$.

372 More precisely, this holds for any $\phi_0 > 0$ such that $|f_A(x) - f_A(y)| < \varepsilon/4$ for
 373 any $x, y \in D$ with $\|x - y\| \leq \phi_0\sqrt{n}/2$.

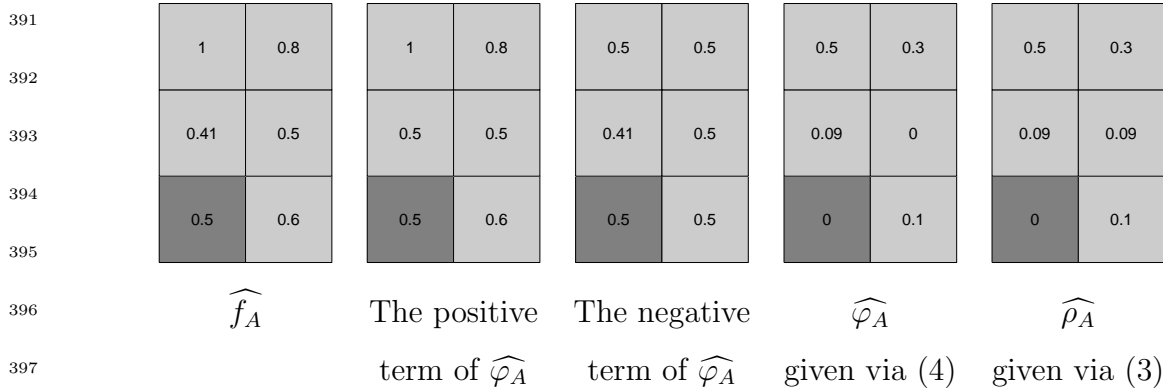
374 *Proof.* Since D is compact and f_A is continuous, f_A is uniformly continuous.
 375 So, there exists a $\phi_0 > 0$ from the last sentence of the theorem. We need to
 376 show that (•) holds for such a ϕ_0 . We will show this only for the operator
 377 ρ_A , the argument for the operator φ_A being similar.

378 To show this, fix $p, q \in \widehat{D}_\phi$. We need to prove that $\widehat{\rho}_A(p, q) < \rho_A(p, q) + \varepsilon$
 379 and $\rho_A(p, q) < \widehat{\rho}_A(p, q) + \varepsilon$. To argue for the first of these inequalities, choose a
 380 $\pi \in \Pi_{p,q}$ for which $\max_t f_A(\pi(t)) - \min_t f_A(\pi(t)) < \rho_A(p, q) + \varepsilon/2$. Let $\widehat{\pi}$ be as
 381 in Remark 2 and let i_0 be such that $\max_i \left[\widehat{f}_A(\widehat{\pi}(i)) \right] = f_A(\widehat{\pi}(i_0))$. Then, there
 382 is a t_0 for which $\|\pi(t_0) - \widehat{\pi}(i_0)\| \leq \phi_0\sqrt{n}/2$. So, $|f_A(\pi(t_0)) - f_A(\widehat{\pi}(i_0))| \leq \varepsilon/4$
 383 and $\max_i \left[\widehat{f}_A(\widehat{\pi}(i)) \right] = f_A(\widehat{\pi}(i_0)) \leq f_A(\pi(t_0)) + \varepsilon/4 \leq \max_t [f_A(\pi(t))] + \varepsilon/4$.
 384 Similarly, we prove that $\min_i \left[\widehat{f}_A(\widehat{\pi}(i)) \right] \geq \min_t [f_A(\pi(t))] - \varepsilon/4$. Hence

385
$$\begin{aligned} \widehat{\rho}_A(p, q) &\leq \max_i \left[\widehat{f}_A(\widehat{\pi}(i)) \right] - \min_j \left[\widehat{f}_A(\widehat{\pi}(j)) \right] \\ &\leq \max_t f_A(\pi(t)) - \min_t f_A(\pi(t)) + \varepsilon/2 < \rho_A(p, q) + \varepsilon/2 + \varepsilon/2, \end{aligned}$$

386 proving $\widehat{\rho}_A(p, q) < \rho_A(p, q) + \varepsilon$. The inequality $\rho_A(p, q) < \widehat{\rho}_A(p, q) + \varepsilon$ is
 387 proved similarly. □

388



398 Figure 4: Values of $\widehat{\rho}_A$ and $\widehat{\varphi}_A$ obtained on a small image. Note the difference between
 399 $\widehat{\rho}_A$ and its approximation $\widehat{\varphi}_A$. The dark gray pixel corresponds to the point with respect
 400 to which the path values are calculated.

401 Since, by Theorem 2, both $\widehat{\rho}_A(p, q)$ and $\widehat{\varphi}_A(p, q)$ converge, as $\phi \rightarrow 0$, to
 402 $\rho_A(p, q) = \varphi_A(p, q)$, we obtain the following corollary.

403 **Corollary 1.** $\max_{p, q \in \widehat{D}_\phi} |\widehat{\rho}_A(p, q) - \widehat{\varphi}_A(p, q)| \rightarrow 0$ as $\phi \rightarrow 0$.

404

405

406 *3.2. The algorithm*

407 Among the two versions of the discrete minimum barrier distance func-
 408 tions, $\widehat{\rho}_A(p, q)$ and $\widehat{\varphi}_A(p, q)$, only the first one is defined as the minimal (ap-
 409 propriately defined) length of a single path from p to q —the feature shared
 410 by essentially all useful distance notions. Because of this property, it is the
 411 function $\widehat{\rho}_A$, rather than $\widehat{\varphi}_A$, that we consider to be the proper definition of
 412 the discrete minimum barrier distance. So, why didn't we stick in this paper
 413 to the discussion $\widehat{\rho}_A$ (and bothered with $\widehat{\varphi}_A$, φ_A , and ρ_A)?

414 An answer is given by Proposition 2(iii): there seems to be no algo-
 415 rithm that efficiently computes the exact value of $\widehat{\rho}_A(p, q)$. To solve this

417 predicament, we turned to finding an efficient algorithm for finding an ap-
418 proximation of $\widehat{\rho}_A$. According to Corollary 1, which combines Theorems 1
419 and 2, the function $\widehat{\varphi}_A$ constitutes an approximation of $\widehat{\rho}_A$. Moreover, $\widehat{\varphi}_A(p, \cdot)$
420 can be found by a Dijkstra's algorithm, which computes each of the terms
421 $\min_{\widehat{\pi}_1 \in \widehat{\Pi}_{p,q}} \max_i \left[\widehat{f}_A(\widehat{\pi}_1(i)) \right]$ and $\max_{\widehat{\pi}_0 \in \widehat{\Pi}_{p,q}} \min_j \left[\widehat{f}_A(\widehat{\pi}_0(j)) \right]$ separately. In
422 particular, the time complexity of such algorithm is $O(N \log N)$, where N is
423 the number of points in the image domain. In what follows, we will use the
424 output of this algorithm as an approximation of $\widehat{\rho}_A$.

425 It is worth to mention, that there are other algorithms with the same
426 computational complexity, that approximate $\widehat{\rho}_A$. For example, in [21], an
427 approximation of $\widehat{\rho}_A$ (for vectorial functions \widehat{f}_A) is found by a version of
428 Dijkstra's algorithm, which propagates according to the path cost function
429 $\max_i \left[\widehat{f}_A(\widehat{\pi}(i)) \right] - \min_j \left[\widehat{f}_A(\widehat{\pi}(j)) \right]$. A similar approach was used in a prelim-
430 inary version of this paper. The experimental results show that the output of
431 such algorithm is very close to $\widehat{\varphi}_A$ (so, it approximates $\widehat{\rho}_A$). However, at the
432 present time, there is no theoretical result (in form of Corollary 1) that the
433 output of such algorithm must approximate $\widehat{\rho}_A$. Thus, so far, $\widehat{\varphi}_A$ constitutes
434 the best approximation of $\widehat{\rho}_A$.

443 **4. The experiments**

444 In this section, we compare the minimum barrier distance $\widehat{\varphi}_A$, approxi-
 445 mating $\widehat{\rho}_A$, with the following distance functions, described in detail below:
 446 fuzzy distance d_F , geodesic distance d_G , and max-arc distance d_{\max} . Having
 447 in mind the applicability of the distance functions in image segmentations, we
 448 will concentrate on examining two desired properties that a distance func-
 449 tion should have: (A) producing the high ratios between the inter-object
 450 distances and the intra-object distances; (B) being relatively unaffected by a
 451 change of the position of seeds (robustness with respect seeds position) and
 452 by an introduction of noise and blur to the image intensity function. There-
 453 fore, our experiments are designed to measure how each of these distances is
 454 influenced by a change of the position of seeds, Figure 5, and an introduction
 455 of noise and blur to the image intensity function, Figures 6 and 7. Notice,
 456 that the study of noise and blur effects give, in particular, an information
 457 of the ratio from (A). All distances we consider ($\widehat{\varphi}_A$, d_F , d_G , and d_{\max}) are
 458 computed by minor variations of Dijkstra wave-front propagation algorithm.
 459 So, the time complexity of each of these algorithms is $O(N \log N)$, where N
 460 is the number of points in the image domain.

461 For each of the distance measures d_F , d_G , and d_{\max} , the distance between
 462 two points, p and q , is defined as the minimal cost of a path between p and
 463 q , where the cost of a path $\langle p_1, p_2, \dots, p_m \rangle$ is defined as follows.

- 464 • For the *fuzzy distance*,

$$465 \sum_{i=1}^{m-1} \frac{f_A(p_i) + f_A(p_{i+1})}{2} \cdot \|p_i - p_{i+1}\|.$$

See [5, 15] for more details. We will also consider the *fuzzy distance on edge* image, where the fuzzy distance is instead applied to an edge image obtained by extracting edges of the image by an edge detection filter. Here, we use gradient magnitude obtained by the Prewitt operator.

- For the geodesic distance d_G

$$\sum_{i=1}^{m-1} \omega |f_A(p_i) - f_A(p_{i+1})| + \|p_i - p_{i+1}\|. \quad (5)$$

See [15, 27] for details. The parameter ω affects trade-off between the fuzzy membership values and the distance on the image scene.¹

- For the *max-arc* distance D_{\max}

$$\max_{i=1, \dots, m-1} \psi(f_A(p_i), f_A(p_{i+1})),$$

where ψ is a function that measures dissimilarity between points in the image. Here, we use $\psi(f_A(p_i), f_A(p_{i+1})) = |f_A(p_i) - f_A(p_{i+1})|$. See [16] for details. The max-arc distance can be seen as a reverse (with respect to the order) of fuzzy connectedness measure with the affinity function ψ . (See e.g. [17, 18, 20].)

¹Formula (5) can be also expressed as $\sum_{i=1}^{n-1} \text{dist}(\langle p_i, \omega f_A(p_i) \rangle, \langle p_{i+1}, \omega f_A(p_{i+1}) \rangle)$, where dist is the taxicab metric, that is, $\text{dist}(\langle x_1, y_1 \rangle, \langle x_2, y_1 \rangle) = \|x_1 - x_2\| + \|y_1 - y_2\|$. In standard analysis courses, the geodesic distance is usually defined with the standard Euclidean distance $\sqrt{\|x_1 - x_2\|^2 + \|y_1 - y_2\|^2}$.

495
 496
 497
 498
 499
 500
 501
 502
 503
 504
 505
 506
 507
 508
 509
 510
 511
 512
 513
 514
 515
 516
 517
 518
 519
 520

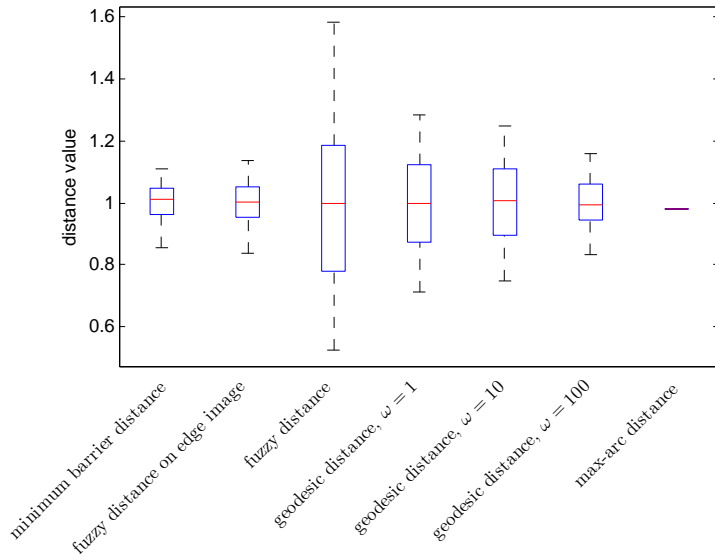
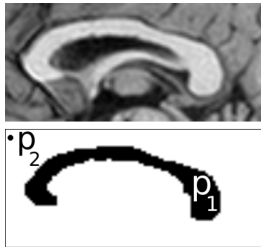
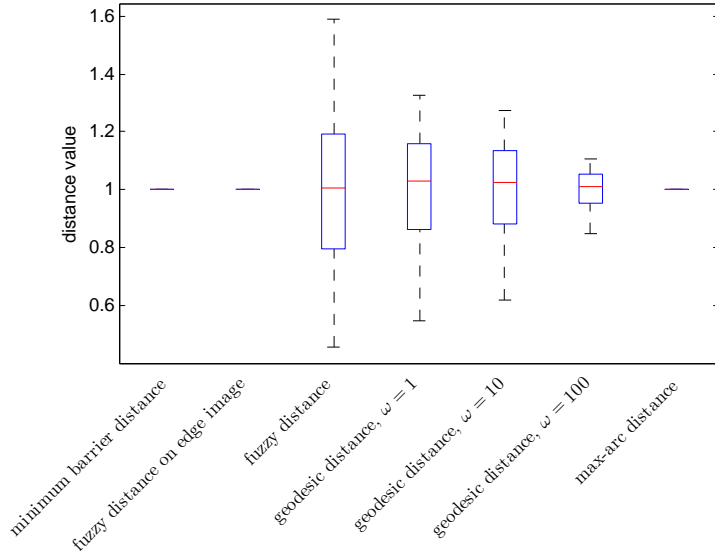
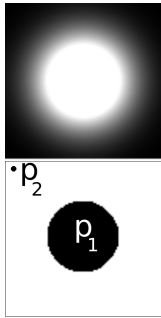
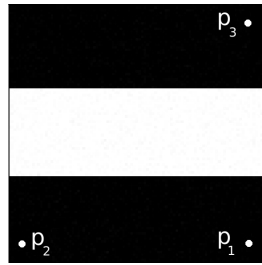


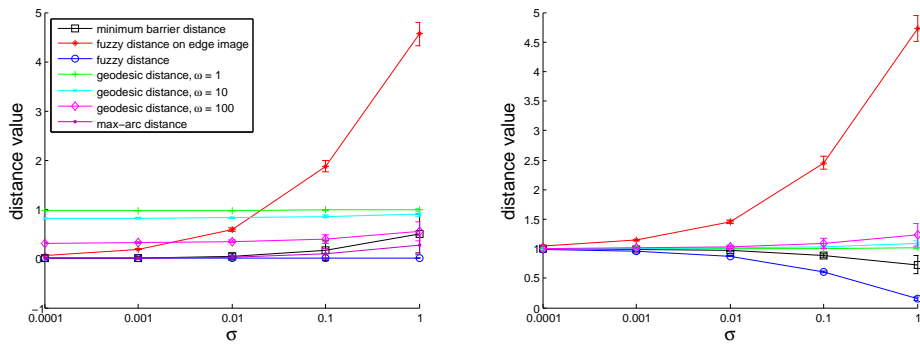
Figure 5: Stability of the distance values $d(p_1, p_2)$ for different distance functions, where the external seed point p_2 is fixed and the the internal seed point p_1 is chosen randomly, within the black region indicated on the left. The distance values are normalized, so that the mean distance value is one. The boxes in the boxplots cover the 25th to the 75th percentile and central mark is the median. The whiskers of the boxplots extend to the most extreme data points not considered outliers.

521
 522
 523
 524
 525
 526
 527
 528
 529
 530
 531
 532
 533
 534
 535
 536
 537
 538
 539
 540
 541
 542
 543
 544
 545
 546



Test image (f_A).

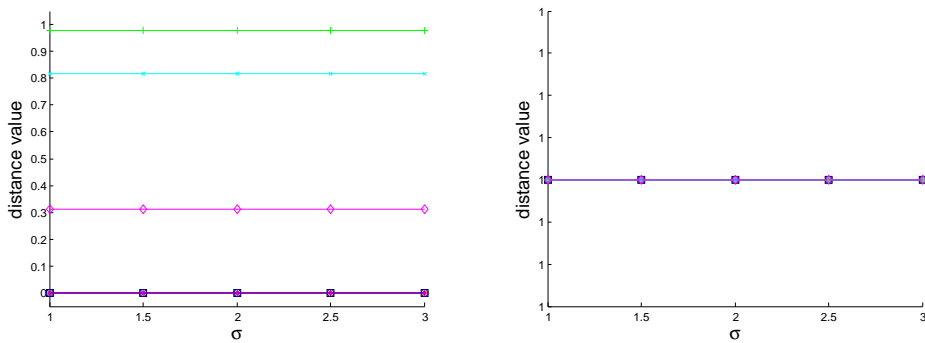
Gaussian noise – Distance values as function of sigma



Intra-object distance ($d(p_1, p_2)$)

Inter-object distance ($d(p_1, p_3)$)

Gaussian smoothing – Distance values as function of sigma

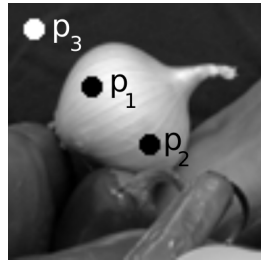


Intra-object distance ($d(p_1, p_2)$)

Inter-object distance ($d(p_1, p_3)$)

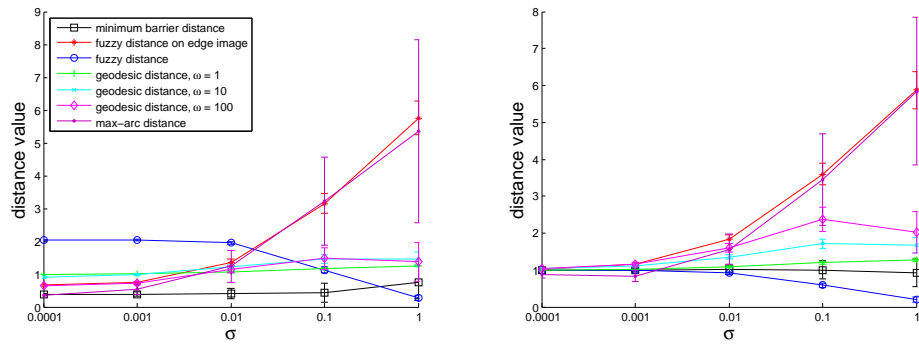
Figure 6: Stability to Gaussian noise and smoothing, see the text. The distance values are normalized so that $d(p_1, p_3) = 1$ on the original image. The confidence intervals in the upper plots cover one standard deviation.

547
548
549
550
551
552
553
554
555
556
557
558
559
560
561
562
563
564
565
566
567
568
569
570
571
572



Test image (f_A).

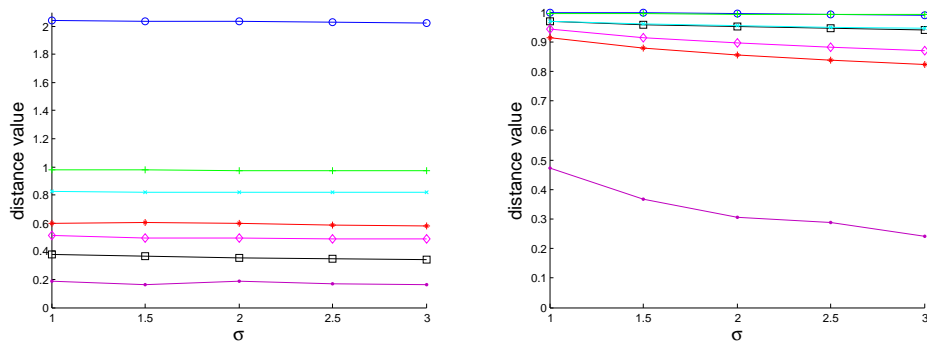
Gaussian noise – Distance values as function of sigma



Intra-object distance ($d(p_1, p_2)$)

Inter-object distance ($d(p_1, p_3)$)

Gaussian smoothing – Distance values as function of sigma



Intra-object distance ($d(p_1, p_2)$)

Inter-object distance ($d(p_1, p_3)$)

Figure 7: Stability to Gaussian noise and smoothing, see the text. The distance values are normalized so that $d(p_1, p_3) = 1$ on the original image. The confidence intervals in the upper plots cover one standard deviation.

573 *4.1. The results*

574 In all experiments we use 2D images considered with the 4-connectedness
575 (α -adjacency). Note that all algorithms are “blind” in the sense that no
576 prior information is considered. Fuzzy connectedness (and therefore max-arc
577 distance), for example, can incorporate an object feature based component
578 with prior information about for example the expected intensity in an object,
579 see [17, 18]. Including such features would require training.

580 *Stability with respect to the seed points position.* To test the different dis-
581 tance functions for its stability with respect to the change of the seed points
582 position, we use two test images presented in each row of Figure 5 as the top
583 image of the left column. The boxplots in Figure 5 show, for each distance
584 function, the distribution of the distance value between a fixed (external)
585 seed point p_2 and, for each of the 1000 repetitions of the experiment, an
586 internal seed point p_1 randomly chosen within the black region indicated on
587 the left of the figure.
588

589 *Stability with respect to noise and smoothing (blur).* The results of the ex-
590 periments are presented, respectively, in Figures 6 and 7. The original tested
591 images are shown at the top of the figures. In the noise experiment, the
592 images are degraded by an additive Gaussian noise with zero mean and vari-
593 ance values of: 0.0001, 0.001, 0.01, 0.1 and 1. For the blur experiment, we
594 use Gaussian smoothing with σ between 0 and 3. The setup is as follows:
595 two inter-object seeds, p_1 and p_2 , and an intra-object seed p_3 are fixed for
596 the entire experiment; (i) Gaussian noise is randomly generated 1000 times
597 for each value of σ ; and (ii) the image is filtered with a Gaussian filter with
598

599 different values of σ . In each iteration, we calculate the inter-object distance
600 between p_1 and p_2 , as well as the intra-object distance between p_1 and p_3 .
601 The distance values are scaled so that the distance between p_1 and p_3 is
602 1 on the original image. The figures show, for each distance function and
603 each distortion, the median of the obtained values as well as the associated
604 confidence interval.

605 *4.2. Interpretation of the experimental results*

606 According to Figure 5, the max-arc distance d_{\max} is by far the most robust
607 with respect to seed choice. This is not surprising, since according to the seed-
608 robustness theorem for fuzzy connectedness, changing a seed p_1 to another
609 seed p'_1 within the same fuzzy connectedness object (defined via d_{\max}) does
610 not affect at all the delineated object. The strong point for the minimum
611 barrier distance is that, from this point of view, the minimum barrier distance
612 is only a bit worse than d_{\max} and far better than other distances we consider.
613

614 The experiments also verify, see Figures 6 and 7, that the minimum barrier
615 distance has, in general, low sensitivity to noise and blur. At the same time,
616 the distances based on gradient magnitude (fuzzy distance on edge image and
617 max-arc distance) are sensitive to noise, see Figure 7. In particular, while
618 the max-arc distance g_{\max} is stable when strong gradients are present, the
619 inter-object g_{\max} distance is not stable against Gaussian smoothing, as can
620 be seen in Figure 7.

621 The positive exception here is the fuzzy distance function, which performs
622 well on the intensity image when the intensities within an object are low
623 and the intensities between different objects are high. This can be seen in
624 Figure 6, where the intensities within an object are low and the intensities

625 between different objects are high, and in Figure 7, where the intensities
626 within the object are high, which results in a high intra-object distance and
627 a low inter-object distance. (The weak performance of the fuzzy distance
628 function is its dependence on seed position, see above.)

629 Finally, notice in Figures 6 and 7, that all considered distances perform
630 reasonably well in separating the object and background, in the sense de-
631 scribed in (A) above. However, as seen in Figure 5, the performance of the
632 max-arc distance g_{\max} is considerably better for the images with the strong
633 gradient and no noise (Figure 6) than when the gradients are weak as in
634 Figure 7. There is no similar drop of performance with this respect for the
635 minimum barrier distance.

636 In summary, the minimum barrier distance function compares favorable
637 with the other distances we compared it with. This make it a good candidate
638 for many many imaging tasks, that use distance functions.

639 5. Conclusions and Future Work

640
641 In this paper we proposed a novel distance function, the minimum barrier
642 distance, which effectively computes the distance values for digital images.
643 It compares favorable with the fuzzy, geodesic, and max-arc distances, when
644 considered is stability with respect to change of seed position and introduc-
645 tion of voice or blur.

646 The main characteristic of the value of minimum barrier distance is based
647 on the image homogeneity, making it robust against weak gradients and
648 noise. This stays in contrast with many other distance functions, used in
649 the wave-front propagation segmentation methods (like watersheds [28, 29])
650

651 and fuzzy connectedness [17, 18]), which are based on gradient information,
652 image inhomogeneity, and so are less robust for noise and do not perform
653 well for the images with weak gradients.

654 In the geodesic distance, the parameter ω in (5) gives the trade-off be-
655 tween the accumulated gradient magnitude along the path and the accu-
656 mulated Euclidean distance between consecutive points. High ω gives low
657 robustness to noise and low ω gives a distance function that is independent
658 of the intensities.

659 Notice that the computational complexity for finding the approximation
660 of the minimum barrier distance $\hat{\varphi}$ is low, since the standard Dijkstra wave-
661 front propagation algorithms can be used. However, to approximate with
662 higher accuracy and precision, we need to increase the resolution. If we need
663 to better approximate ρ , this could mean a substantial increase in computa-
664 tional complexity. We note that subsampling is not needed in homogenous
665 regions.

666 In our future work, we plan to make local approximations in regions
667 where the inhomogeneity of f_A is high. In this way we think that we will
668 achieve better approximation without significant increase in computational
669 complexity. We also plan to examine the case with multiple seed points in
670 our future work.

671 We believe that this method has the potential of being useful in many
672 applications where homogeneous regions are extracted, for example segmen-
673 tation.

677 **Acknowledgement**

678 We thank the anonymous reviewers for their insightful comments that
679 helped us to improve this manuscript.
680

681 **References**

- 682 [1] A. Rosenfeld, J. L. Pfaltz, Distance functions on digital pictures, *Pattern*
683 *Recognition* 1 (1968) 33–61.
684
- 685 [2] G. Borgefors, Distance transformations in arbitrary dimensions, *Com-*
686 *puter Vision, Graphics, and Image Processing* 27 (1984) 321–345.
- 687 [3] G. Borgefors, On digital distance transforms in three dimensions, *Com-*
688 *puter Vision and Image Understanding* 64 (3) (1996) 368–376.
689
- 690 [4] P.-E. Danielsson, Euclidean distance mapping, *Computer Graphics and*
691 *Image Processing* 14 (1980) 227–248.
- 692 [5] P. K. Saha, F. W. Wehrli, B. R. Gomberg, Fuzzy distance transform:
693 theory, algorithms, and applications, *Computer Vision and Image Un-*
694 *derstanding* 86 (2002) 171–190.
- 695 [6] R. Strand, Distance functions and image processing on point-lattices:
696 with focus on the 3D face- and body-centered cubic grids, Ph.D. thesis,
697 Uppsala University, Sweden,
698 <http://urn.kb.se/resolve?urn=urn:nbn:se:uu:diva-9312> (2008).
699
- 700 [7] R. Strand, B. Nagy, G. Borgefors, Digital distance functions on three-
701 dimensional grids, *Theoretical Computer Science* 412 (15) (2011) 1350
702 – 1363.

- 703 [8] T. Hildebrand, P. Rügsegger, A new method for the model-independent
704 assessment of thickness in three-dimensional images, *Journal of Mi-*
705 *croscopy* 185 (1) (1997) 67–75.
- 706 [9] P. K. Saha, Z. Gao, S. K. Alford, M. Sonka, E. A. Hoffman, Topomor-
707 phologic separation of fused isointensity objects via multiscale opening:
708 Separating arteries and veins in 3-D pulmonary CT, *IEEE Transactions*
709 *on Medical Imaging* 29 (3) (2010) 840–851.
- 710 [10] P. K. Saha, F. W. Wehrli, Measurement of trabecular bone thickness in
711 the limited resolution regime of in vivo MRI by fuzzy distance transform,
712 *IEEE Transactions on Medical Imaging* 23 (1) (2004) 53–62.
- 713 [11] A. Rosenfeld, J. L. Pfaltz, Sequential operations in digital picture pro-
714 cessing, *Journal of the ACM* 13 (4) (1966) 471–494.
- 715 [12] Maurer, C.R., Jr., Qi, R., and Raghavan, V.: A linear time algorithm
716 for computing exact Euclidean distance transforms of binary images
717 in arbitrary dimensions, *IEEE Transactions on Pattern Analysis and*
718 *Machine Intelligence* 25 (2) (2003), 265–270.
- 719 [13] K. C. Ciesielski, X. Chen, J. K. Udupa, G. J. Grevera Linear time al-
720 gorithm for exact distance transform, *Journal of Mathematical Imaging*
721 *and Vision* 39 (3) (2011), 193–209.
- 722 [14] J. A. Sethian, *Level Set Methods and Fast Marching Methods*, Cam-
723 bridge University Press, 1999.
- 724 [15] C. Fouard, M. Gedda, An objective comparison between gray weighted
725 distance transforms and weighted distance transforms on curved spaces,
726
727
728

- 729 in: A. Kuba, L. G. Nyúl, K. Palágyi (Eds.), Discrete Geometry for
730 Computer Imagery, 13th International Conference, DGCI 2006, Szeged,
731 Hungary, October 25-27, 2006, Proceedings, Vol. 4245 of Lecture Notes
732 in Computer Science, Springer, 2006, pp. 259–270.
- 733 [16] A. X. Falcão, J. Stolfi, R. de Alencar Lotufo, The image foresting trans-
734 form: Theory, algorithms, and applications, IEEE Transactions on Pat-
735 tern Analysis and Machine Intelligence 26 (1) (2004) 19–29.
- 736 [17] J. K. Udupa, P. K. Saha, R. A. Lotufo, Relative fuzzy connectedness
737 and object definition: Theory, algorithms, and applications in image
738 segmentation, IEEE Transactions on Pattern Analysis and Machine In-
739 telligence 24 (2002) 1485–1500.
- 740 [18] J. K. Udupa, P. K. Saha, Fuzzy connectedness and image segmentation,
741 Proceedings of the IEEE 91 (10) (2003) 1649 – 1669.
- 742 [19] A. Rosenfeld, Fuzzy digital topology, Information and Control 40 (1)
743 (1979) 76 – 87.
- 744 [20] K. C. Ciesielski, J. K. Udupa, A framework for comparing different im-
745 age segmentation methods and its use in studying equivalences between
746 level set and fuzzy connectedness frameworks, Computer Vision and
747 Image Understanding 115 (6) (2011) 721–734.
- 748 [21] A. Kårsnäs, R. Strand, P. K. Saha, The Vectorial Minimum Barrier
749 Distance, Proceedings of the 21st International Conference on Pattern
750 Recognition, November 2012, Japan. Accepted.
- 751
752
753
754

- 755 [22] M. H. A. Newman, Elements of the Topology of Plane Sets of Points,
756 Cambridge, 1964.
- 757 [23] T. Y. Kong, A. Rosenfeld, Digital topology: introduction and survey,
758 Computer Vision, Graphics, and Image Processing 48 (3) (1989) 357–
759 393.
- 760 [24] U. Köthe, What Can We Learn from Discrete Images about the Con-
761 tinuous World?, in: D. Coeurjolly, I. Sivignon, L. Tougne, F. Dupont
762 (Eds.), Discrete Geometry for Computer Imagery, 14th International
763 Conference, DGCI 2008, Lyon, France, 2008, Proceedings, Vol. 4992 of
764 Lecture Notes in Computer Science, Springer, 2008, pp. 4–19.
- 765 [25] P. Stelldinger, Topologically correct 3D surface reconstruction and seg-
766 mentation from noisy samples, in: V. Brimkov, R. Barneva, H. Haupt-
767 man (Eds.), Proceedings of the 12th international conference on Combi-
768 natorial image analysis, Vol. 4958 of Lecture Notes in Computer Science,
769 Springer-Verlag, Berlin, Heidelberg, 2008, pp. 274–285.
- 770 [26] E. Dougherty, R. Lotufo, Hands-on morphological image processing, Tu-
771 torial texts in optical engineering, SPIE Press, 2003.
- 772 [27] P. J. Toivanen, New geodesic distance transforms for gray-scale images,
773 Pattern Recognition Letters 17 (1996) 437–450.
- 774 [28] L. Vincent, P. Soille, Watersheds in digital spaces: an efficient algorithm
775 based on immersion simulations, IEEE Transactions on Pattern Analysis
776 and Machine Intelligence 13 (6) (1991) 583 –598.
- 777
778
779
780

781 [29] P. Soille, Morphological Image Analysis: Principles and Applications,
782 2nd Edition, Springer-Verlag New York, Inc., Secaucus, NJ, USA, 2003.

783

784

785

786

787

788

789

790

791

792

793

794

795

796

797

798

799

800

801

802

803

804

805

806